

## THE TERBIUM-ANTIMONY ALLOY SYSTEM

M. N. ABDUSALYAMOVA, O. R. BURNASHEV and K. E. MIRONOV

*Institute of Chemistry of the Academy of Sciences of the Tajik S.S.R., Dushanbe-63, 734063 (U.S.S.R.)*

(Received March 24, 1980)

### Summary

A phase diagram is proposed for the Tb-Sb system on the basis of differential thermal, X-ray, chemical and microscopy analyses. A peritectic reaction develops as a result of antimony additions and the transformation temperature of terbium is lowered by 25 °C. Eutectic reactions occur at 14 at.% Sb and 1130 °C and at greater than 99.0 at.% Sb and 623 °C. There are four compounds in the system:  $Tb_5Sb_3$  and  $Tb_4Sb_3$  result from peritectic reactions at 1650 and 1770 °C while TbSb melts congruently at 2160 °C. The overall phase homogeneity range is no more than 1 at.%. Results for the formation of  $TbSb_2$  at normal pressures are reported.  $Tb_4Sb_3$  and TbSb were observed to exhibit polymorphic transformations.

---

### 1. Introduction

The purpose of this work was to study phase relationships in the Tb-Sb system and to propose a phase diagram. This investigation is a part of our research on the interaction of the rare earth metals with antimony and bismuth and on the properties of the compounds formed.

Three compounds between terbium and antimony have previously been reported:  $Tb_5Sb_3$  with the  $Mn_5Si_3$  structure [1],  $Tb_4Sb_3$  with the anti- $Th_3P_4$  structure [2, 3] and TbSb with the NaCl structure [4, 5]. Eatough and Hall [6] have found that the application of high pressure yields two  $TbSb_2$  modifications.

### 2. Experimental procedures

#### 2.1. Materials

Terbium distillate TbMD-2 (Table 1) and antimony of semiconducting purity SCH-0000 were used for the investigation.

TABLE 1

The impurity concentrations in terbium TbMD-2

Impurity Concentration (at.%)	C	Ca	Dy, Y, Gd	Cu	Fe	Si	H <sub>2</sub>	F	N <sub>2</sub>
	0.003	0.004	<0.05	<0.01	<0.01	<0.01	<0.002	<0.004	0.008

### 2.2. Alloy preparation

27 compositions in the concentration range 0 - 50 at.% Sb and 12 compositions in the range 50 - 100 at.% Sb were prepared for the investigation. Each composition investigated was prepared in duplicate or triplicate and differential thermal analysis (DTA) of the samples was carried out in parallel. The alloys were formed from stoichiometric amounts of the powdered components placed inside evacuated ampoules of molybdenum glass which were heated in a resistance furnace. A slow step-by-step temperature increase was used to reach 500 °C in 60 h. The ampoules were held at this temperature for 2 days. The products were ground in a mortar and were formed into pellets. Homogeneity was obtained by heating the pellet in a crucible with a lid up to a temperature well above the liquidus in an atmosphere of very pure helium. The same technique was used for both the homogeneous annealing and the thermal analysis procedures.

### 2.3. Thermal analysis

A high temperature differential thermal analyser (WDTA, U.S.S.R.) [7] was used for the DTA measurements which were made in very pure helium (99.985 vol.% He). The heating and cooling rates were both 30 °C min<sup>-1</sup>. A high temperature sensor with string W/W-20%Re thermocouples [8] was used for temperature measurements.

The thermocouple was calibrated at the melting points of the following superpure metals and oxides: tin, 231.8 °C; bismuth, 271.3 °C; lead, 327.4 °C; zinc, 419.5 °C; antimony, 630.5 °C; aluminium, 660.0 °C; silver, 960 °C; copper, 1083 °C; nickel, 1453 °C; iron, 1539 °C; platinum, 1769 °C; vanadium, 1950 °C; Al<sub>2</sub>O<sub>3</sub>, 2042 °C; Sm<sub>2</sub>O<sub>3</sub>, 2325 °C; Y<sub>2</sub>O<sub>3</sub>, 2410 °C. The temperature was accurate to within ±1% of the measured value. The temperatures for the reactions were read from the heating curves since most of the alloys had an increased tendency to supercooling. Thermograms of the temperature of the sample against the difference between the temperatures of the sample and the standard specimen were obtained; the standard specimen was made of molybdenum. Tantalum crucibles were used for the DTA of samples containing up to 55 at.% Sb. Molybdenum or alumina crucibles were used for the investigation of antimony-rich alloys as tantalum has considerable solubility in liquid antimony.

Sealed crucibles were used for the antimony-rich alloys to exclude antimony losses due to sublimation. A thin-walled molybdenum or alumina crucible was mounted inside a crucible made of tantalum, the latter being

sealed with a tantalum cone cap. Such a crucible design completely excludes antimony losses during DTA. Because the crucibles for the samples with up to 55 at.% Sb were unsealed, it was necessary to check the samples for composition by weighing the crucibles just before and just after heating as well as by chemical and X-ray fluorescence analyses. The weight losses of a 1.5 g sample did not exceed 10 mg. The sample was analysed chemically for terbium, and the deviation from the starting composition did not exceed 0.6 at.%. A VRA-2 X-ray fluorescence spectrometer made in the G.D.R. was also used. The data obtained revealed no deviation from the starting composition, the error in the measurements being no more than 1 at.%.

#### 2.4. X-ray method

The X-ray analysis was carried out with Cu K $\alpha$  radiation using a TUR-M62 diffractometer with an HCG-3 goniometer made in the G.D.R. Both powders and bulk materials were used for these analyses which were carried out after the DTA.

#### 2.5. Microscopy analysis

Microstructures were studied and photographs were taken with an MIM-8 microscope with both ordinary and polarized light. A PMT-3 apparatus was used for microhardness measurements. Both items of equipment were made in the U.S.S.R. The samples were prepared from bulk compact materials after the DTA measurements had been performed. Diamond discs were used for grinding and polishing. For structure identification and for cold work removal the samples were etched in a solution of 2 wt.% HNO<sub>3</sub> in ethanol or by exposing them in air for several hours. The microhardness measurements were carried out by 20 gf loading on separate grains for each phase.

### 3. Results and discussion

The results of the investigation by all the methods described in Section 2 are summarized in the Tb-Sb phase diagram (Fig. 1) Some details of the antimony-rich part of the diagram are discussed later (see Fig. 4). The DTA procedure was used to determine the invariant horizontals associated with the inverse peritectic and eutectic reactions and to determine the liquidus position. The phase diagram boundaries were confirmed by microscopy, X-ray, chemical and X-ray fluorescence methods.

#### 3.1. Inverse peritectic and eutectic reactions

An inverse peritectic reaction occurs at the terbium-rich end of the system at  $1265 \pm 10$  °C and at approximately 1 at.% Sb. The evidence for this reaction was obtained from the heating and cooling curves which showed a decrease of approximately 25 °C in the  $\alpha$ -Tb  $\rightleftharpoons$   $\beta$ -Tb transformation; this decrease was caused by antimony additions.

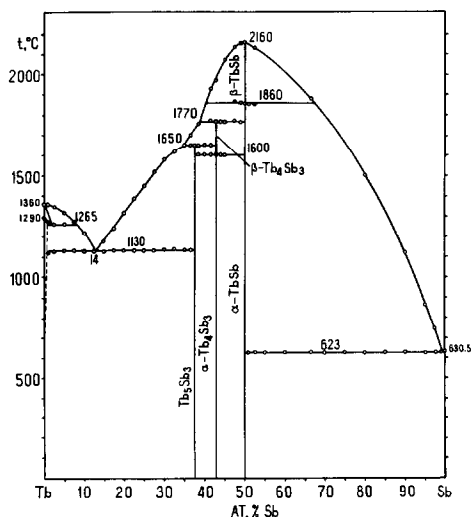


Fig. 1. The Tb-Sb phase diagram and a plot of the thermal analysis data.

A eutectic event occurs on the DTA curve of the sample with a content of 1 at.% Sb. Hence, the antimony solubility in terbium is less than 1 at.%. This is also confirmed by the microstructure analysis data (Fig. 2(a)). Eutectic events are observed on the DTA curves of all the samples in the range 1 - 36.5 at.% Sb, as is indicated by the thermal data plotted in Fig. 1. Only two phases were detected by the microscopy (Figs. 2(b) and 2(c)) and X-ray (Figs. 3(a), 3(b) and 3(c)) analyses in the range 0 - 37.5 at.% Sb, *i.e.*  $\alpha$ -Tb and  $Tb_5Sb_3$ . Thus  $Tb_5Sb_3$  is the most terbium-rich antimonide phase in the system. The eutectic composition corresponds to 14 at.% Sb and is obtained from a Tamman construction. This composition was also substantiated by the metallographic data.

The melting point of antimony is lowered about 7 °C by small terbium additions; this is interpreted as indicating a eutectic reaction at 623 °C. The decrease was detected using the DTA method in which a sample of pure antimony was used as a standard specimen. The microscopy data show that the eutectic composition is greater than 99.0 at.% Sb.

### 3.2. Intermetallic compounds

Three intermetallic compounds having the formulae  $Tb_5Sb_3$ ,  $Tb_4Sb_3$  and  $TbSb$  were identified in the Tb-Sb system. There is also evidence for the existence of  $TbSb_2$ . The data for the compounds together with their structures and melting points are summarized in the following sections.

#### 3.2.1. $Tb_5Sb_3$ (37.5 at.% Sb)

$Tb_5Sb_3$  melts incongruently at  $1650 \pm 15$  °C and crystallizes with the  $Mn_5Si_3$  structure. Crystallographic and microhardness data for this phase are summarized in Table 2. The lattice parameters of  $Tb_5Sb_3$  agree well with

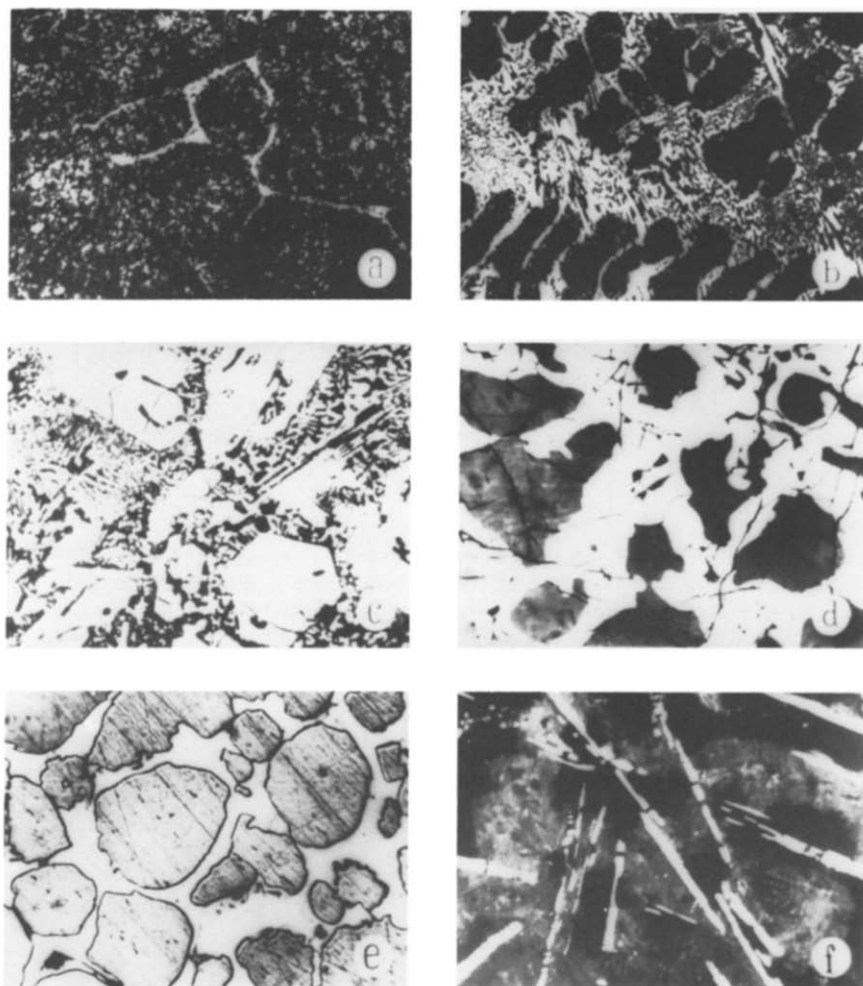


**Fig. 2. Microphotographs for the Tb–Sb alloy system: (a) 1 at.% Sb; dark phase,  $\alpha$ -Tb; light phase,  $Tb_5Sb_3$  (magnification, 250 $\times$ ); (b) 10 at.% Sb; dark crystals of  $\alpha$ -Tb and the eutectic (magnification, 180 $\times$ ); (c) 25 at.% Sb; light crystals of  $Tb_5Sb_3$  and the eutectic (magnification, 200 $\times$ ); (d) 40 at.% Sb; dark crystals of  $\alpha$ - $Tb_4Sb_3$  in a  $Tb_5Sb_3$  matrix (magnification, 180 $\times$ ); (e) 47.5 at.% Sb; grey crystals of  $\alpha$ -TbSb in an  $\alpha$ - $Tb_4Sb_3$  matrix (magnification, 200 $\times$ ); (f) 66.7 at.% Sb; dark crystals of  $\alpha$ -TbSb in an antimony matrix and needle-shaped crystals of  $TbSb_2$  (magnification, 150 $\times$ ).**

those obtained by Rieger and Parthé [1]. The X-ray diagram of the compound with an antimony content of 37.5 at.% is given in Fig. 3(d).

### 3.2.2. $Tb_4Sb_3$ (42.86 at.% Sb)

$Tb_4Sb_3$  forms peritectically at  $1770 \pm 15$  °C and crystallizes with the cubic anti- $Th_3P_4$  structure. The lattice parameter and the microhardness data are presented in Table 2. The value of the lattice parameter agrees well with that given by Hohnke and Parthé [3]. Gambino [2] failed to obtain pure

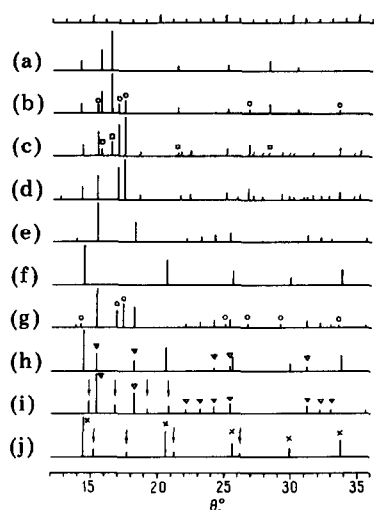


Fig. 3. X-ray diagrams for the Tb-Sb alloy system: (a)  $\alpha$ -Tb (metallic); (b) 10 at.% Sb; (c) 25 at.% Sb; (d) 37.5 at.% Sb; (e) 42.8 at.% Sb; (f) 50 at.% Sb; (g) 40 at.% Sb; (h) 47.5 at.% Sb; (i) 42.8 at.% Sb (annealed at 1650 °C and quenched); (j) 50 at.% Sb (annealed at 1900 °C and quenched). ( $\square$ ,  $\alpha$ -Tb;  $\circ$ ,  $\text{Tb}_5\text{Sb}_3$ ;  $\nabla$ ,  $\alpha$ - $\text{Tb}_4\text{Sb}_3$ ;  $\times$ ,  $\alpha$ -TbSb.)

TABLE 2

Crystallographic data and microhardness values for the phases of the Tb-Sb alloy system

Compound	Crystal system	Structure type	Space group	Parameters <sup>a</sup> (Å)		Microhardness (kgf mm <sup>-2</sup> )
				$a_0$	$c_0$	
$\text{Tb}_5\text{Sb}_3$	Hexagonal	$\text{Mn}_5\text{Si}_3$	$P6_3/mcm$	8.919	6.302	485 ± 20
$\text{Tb}_4\text{Sb}_3$	Cubic	Anti- $\text{Th}_3\text{P}_4$	$I\bar{4}3d$	7.170	—	505 ± 20
TbSb	Cubic	NaCl	$Fm\bar{3}m$	6.178	—	122 ± 7

<sup>a</sup>These parameters are accurate to within  $\pm 0.005$  Å.

$\text{Tb}_4\text{Sb}_3$ . We managed to obtain rather pure  $\text{Tb}_4\text{Sb}_3$ ; the X-ray diagram is given in Fig. 3(e).

### 3.2.3. TbSb (50.0 at.% Sb)

This compound was found to melt congruently at  $2160 \pm 20$  °C and is the highest melting phase in the system. Parameter values reported previously by Brixner [4] and Iandelli [5] agree well with our data (see Table 2). The X-ray diagram of TbSb is given in Fig. 3(f).

In both the ranges 37.5 - 42.9 at.% Sb and 42.9 - 50.0 at.% Sb only two phases were determined, namely  $\text{Tb}_5\text{Sb}_3$  and  $\text{Tb}_4\text{Sb}_3$  (Figs. 2(d) and 3(g)) and  $\text{Tb}_4\text{Sb}_3$  and TbSb (Figs. 2(e) and 3(h)) respectively.

### 3.2.4. $TbSb_2$ (66.67 at.% Sb)

An investigation of  $TbSb_2$  formation has been reported by Eatough and Hall [6] who obtained two modifications, both of which appeared to be stable under normal conditions after quenching. Eatough and Hall have presented a diagram with a range in which "unknown products, type 1" exist together with  $TbSb$ . This range lies below 800 °C and 30 kbar. However, the lower pressure and temperature limits are not given. There is also no suggestion for stoichiometry of the "unknown products". As the starting admixture in the experiments of Eatough and Hall [6] contained terbium and antimony with a stoichiometry of 1:2, after  $TbSb$  formation the remaining products seemed to be either elemental antimony or a composition close to the diantimonide (no evidence for transformation was obtained). The existence of several phases in this range may be due to the short synthesis time (the products were prepared in only 3 min).

The DTA curves in our experiments for alloys containing 52.5 - 95 at.% Sb exhibit events at  $740 \pm 10$  °C as well as the eutectic events. The apex of the Tamman triangle corresponds to  $TbSb_2$  (Fig. 4) which gives us evidence for  $TbSb_2$  formation under normal conditions. In fact the microscopy analysis in the range 52.5 - 95 at.% Sb revealed needle-shaped crystals in the antimony matrix as well as the primary crystals.

In an investigation of the Y-Sb system Schmidt and McMasters [9] observed needle-shaped crystals which have been ascribed to  $TaSb_2$ . As described in Section 2.3, we used molybdenum or alumina crucibles for the experiments relating to the antimony-rich end of the system to exclude  $TaSb_2$  formation.

Figure 2(f) shows a microphotograph of the alloy obtained after a DTA carried out in an  $Al_2O_3$  crucible; the needle-shaped crystals of the third phase can be seen. X-ray analysis revealed several new lines on the diffraction diagram; the nature of these lines is still unknown. However, taking all of these data into account, the antimony-rich end of the diagram seems to correspond to the picture given by Fig. 4. A part of the eutectic line in the range 50.0 - 66.7 at.% Sb (the broken line in Fig. 4) seems to be non-equilibrium because of a slow  $TbSb$ -to- $TbSb_2$  transformation at this low temperature; this follows from our experiments.

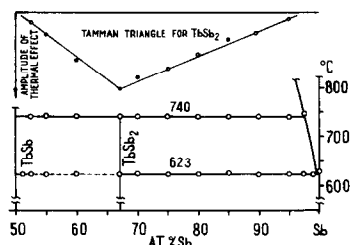


Fig. 4. The antimony-rich end of the Tb-Sb system.

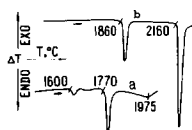


Fig. 5. Thermograms for the Tb-Sb alloy system: curve a, for a composition close to  $Tb_4Sb_3$ ; curve b, for a composition close to TbSb.

### 3.3. Polymorphic transformations of $Tb_4Sb_3$ and TbSb

In DTA curves of the alloys containing  $Tb_4Sb_3$  and TbSb the melting events of these phases are always preceded by sharp events at 1600 °C and 1860 °C respectively (Fig. 5). On cooling these events are reproduced with a slight supercooling. The diffraction patterns of  $Tb_4Sb_3$  and TbSb plotted at temperatures a little below 1600 °C and 1860 °C respectively seem to have additional reflections. These reflections also occur after annealing and quenching of the samples from above 1600 °C and 1860 °C respectively (Figs. 3(i) and 3(j)). We believe that these reflections do not refer either to any of the phases given in Table 2 or to the pure components or their oxides. Thus the existence of polymorphic transformations in  $Tb_4Sb_3$  and TbSb at  $1600 \pm 15$  °C and  $1860 \pm 20$  °C respectively is established from the DTA and X-ray data. We designate the high temperature phases as  $\beta$ - $Tb_4Sb_3$  and  $\beta$ -TbSb. The polymorphic transformation data have not previously been observed. However, Hulliger [10] has shown that monoantimonides have a high temperature modification of the CsCl type.

### Acknowledgments

We thank I. P. Adamchuk and V. I. Weinberg for carrying out the X-ray fluorescence analyses, and E. D. Popova for providing the chemical control of the sample compositions. We also thank V. P. Garmasheva, T. P. Rogozhina, R. V. Nigmatullin and A. A. Pavlovich for technical assistance.

### References

- 1 W. Rieger and E. Parthé, *Acta Crystallogr.*, **24** (1968) 456.
- 2 R. J. Gambino, *J. Less-Common Met.*, **12** (1967) 344.
- 3 D. Hohnke and E. Parthé, *Acta Crystallogr.*, **24** (1968) 435.
- 4 L. H. Brixner, *J. Inorg. Nucl. Chem.*, **15** (1960) 199.
- 5 A. Iandelli, in E. V. Kleber (ed.), *Rare Earth Research*, Macmillan Co., New York, 1961, pp. 135 - 141.
- 6 N. L. Eatough and H. T. Hall, *Inorg. Chem.*, **8** (7) (1969) 1439.
- 7 Yu. A. Kocherzhinsky, N. A. Bezhtanyko, V. I. Vasilenko, A. D. Yevprev, V. G. Yepifanov, A. V. Zakilinski, V. E. Isyanov, B. G. Naumchenko, A. V. Pugach, L. V. Remisovski, V. P. Skvorchuk, V. G. Shestopalov and E. A. Shishkin, *Izv. Sib. Otd. Akad. Nauk S.S.S.R., Ser. Khim. Nauk*, **9** (4) (1974) 32.
- 8 Yu. A. Krakovetsky-Kocherzhinsky, *avt. svid. N 231863*, January 30, 1964; *Izobreteniya, Promyshlennye Obraztzy, Tovarnye Znaki*, **36** (1968) 99.
- 9 F. A. Schmidt and O. D. McMasters, *J. Less-Common Met.*, **21** (1970) 415.
- 10 F. Hulliger, *J. Magn. Magn. Mater.*, **8** (1978) 183.